Targeted degradation of hexokinase 2 for anti-inflammatory treatment in acute lung injury

JIAYAN YANG[1*], LIANGLIANG DONG[2*], YIFAN WANG[3], LIFEN GONG[3], HONGWEI GAO[1] and YICHENG XIE[3]

[1]College of Pharmacy, Guangxi University of Chinese Medicine, Nanning, Guangxi Zhuang Autonomous Region 530000; [2]Department of Pulmonology, Sir Run Run Shaw Hospital, Zhejiang University School of Medicine, Hangzhou, Zhejiang 310016; [3]Department of Pulmonology, Children's Hospital, National Clinical Research Center for Child Health, Zhejiang University School of Medicine, Hangzhou, Zhejiang 310052, P.R. China

Received August 7, 2023; Accepted February 8, 2024

DOI: 10.3892/mmr.2024.13206

Abstract. Acute lung injury (ALI) is an acute inflammatory lung disease associated with both innate and adaptive immune responses. Hexokinase 2 (HK2) is specifically highly expressed in numerous types of inflammation-related diseases and models. In the present study *in vitro* and *in vivo* effects of targeted degradation of HK2 on ALI were explored. The degradation of HK2 by the targeting peptide TAT (transactivator of transcription protein of HIV-1)-ataxin 1 (ATXN1)-chaperone-mediated autophagy-targeting motif (CTM) was demonstrated by ELISA and western blotting *in vitro* and *in vivo*. The inhibitory effects of TAT-ATXN1-CTM on lipopolysaccharide (LPS)-induced inflammatory responses were examined using ELISAs. The therapeutic effects of TAT-ATXN1-CTM on LPS-induced ALI were examined via histological examination and ELISAs in mice. 10 μM TAT-ATXN1-CTM administration decreased HK2 protein expression and the secretion of proinflammatory cytokines (TNF-α and IL-1β) without altering HK2 mRNA expression in LPS-treated both *in vitro* and *in vivo*, while pathological lung tissue damage and the accumulation of leukocytes, neutrophils, macrophages and lymphocytes in ALI were also significantly suppressed by 10 μM TAT-ATXN1-CTM treatment. TAT-ATXN1-CTM exhibited anti-inflammatory activity *in vitro* and decreased the severity of ALI *in vivo*. HK2 degradation may represent a novel therapeutic approach for ALI.

Correspondence to: Dr Hongwei Gao, College of Pharmacy, Guangxi University of Chinese Medicine, 13 Wuhe Avenue, Nanning, Guangxi Zhuang Autonomous Region 530000, P.R. China
E-mail: gaohongwei06@126.com

Dr Yicheng Xie, Department of Pulmonology, Children's Hospital, National Clinical Research Center for Child Health, Zhejiang University School of Medicine, 3333 Binsheng Road, Hangzhou, Zhejiang 310052, P.R. China
E-mail: ycxie@zju.edu.cn

*Contributed equally

Key words: acute lung injury, hexokinase 2, transactivator of transcription protein of HIV-1-ataxin 1-chaperone-mediated autophagy-targeting motif

Introduction

Acute lung injury (ALI) is an acute inflammation characterized by pulmonary hemorrhage, increased vascular permeability and inflammatory cell infiltration (1). In severe cases, it may even lead to acute respiratory failure and death (2). According to reports, the incidence of ALI (~200,000 cases per year in the United States) and the overall mortality rate remain high, with ALI also being a prevalent cause of morbidity and mortality in critically ill patients (2,3). Although the understanding of the pathogenesis of ALI has improved, there is still no effective drug therapy to reduce the mortality rates of patients with ALI (4). Bacterial lipopolysaccharide (LPS) infection is one of the most common causes of ALI (5), by triggering inflammatory signal transduction, resulting in excessive production of cytokines such as IL-1β and TNF-α, creating an inflammatory storm (6). It has been demonstrated that inhibiting the excessive inflammatory cascade reaction of ALI is an effective strategy to reduce lung injury (7). Therefore, controlling the inflammatory response is a key measure for the prevention and treatment of ALI.

Macrophages serve as the first line of defense against the lung invasion of pathogens and are critical in initiating and maintaining inflammatory responses, reducing inflammation and restoring lung function (8). Previous studies have demonstrated that glycolysis in macrophages increased during lung inflammation and that inhibiting glycolysis could alleviate lung inflammation (9,10). For instance, the glycolysis inhibitor, 2-deoxy-D-glucose (2-DG) reduces triggering receptor expressed on myeloid cells 1-triggered activation of the NLR family pyrin domain containing 3 (NLRP3) inflammasome in lung macrophages (11).

As the first rate-limiting enzyme of glycolysis, hexokinase (HK) catalyzes the conversion of glucose into glucose-6-phosphate (G-6P). There are four subtypes of HK in mammals, namely HK1-4, and the distribution of the four HKs in the mammalian body is also different, with tissue and cell specificity (12). The HK subtypes distributed in the lungs

are dominated by HK1 and HK2, with HK1 tending to be expressed in healthy tissues, whereas HK2 is more effective than the other subtypes in promoting aerobic glycolysis (13,14), supporting the involvement of HK2 in the regulation of pulmonary disorders. Therefore, HK2 may be a more promising target. Previous studies have suggested that HK2 is less extensively distributed and expressed in healthy tissues but is specifically highly expressed in various inflammation-related diseases and models, suggesting the involvement of HK2 in regulating immune responses (12,15). Therefore, it was hypothesized that selective inhibition of HK2 can regulate the release of inflammatory factors in lung macrophages with less impact on system stability and body metabolism. In conclusion, reducing the inflammatory response by inhibiting HK2 activity may be a potential strategy for the treatment of ALI. However, to the best of our knowledge, highly selective HK2 inhibitors have not been reported for the treatment of ALI.

The existing commonly used HK2 inhibitors have high rates of adverse reactions due to their low specificity (16). Currently, the most commonly used HK2 inhibitors in preclinical studies are lonidamine, 2-DG and 3-bromopyruvate, all of which are antitumor drugs that stem tumor progression by suppressing glycolysis (17,18). There is a high degree of homology between HK1 and HK2, and given the wide distribution and important functions of HK1, these HK2 inhibitors are likely to inhibit HK1 activity while inhibiting HK2 activity (19,20).

To explore novel therapeutic strategies, the present study attempted to reduce HK2 protein levels by chaperone-mediated autophagy (CMA) (21). CMA is a critical pathway in lysosomes for the specific degradation of unnecessary proteins, particularly serving a pivotal role in clearing misfolded proteins (22). Therefore, using the lysosomal system to target the degradation of pathogenic proteins may be an effective strategy to address diseases. CMA-targeted chimeras are a class of molecules designed using the CMA system, usually consisting of a cell-penetrating peptide (TAT, transactivator of transcription protein of HIV-1), target protein-binding domain (PBD) and CMA-targeting motif (CTM) (23). Therefore, a targeting peptide [TAT-ataxin 1 (ATXN1)-CTM] was synthesized based on the knowledge that ATXN1 protein can bind HK2 protein. Mechanistically, the peptide can interact with the endogenous HK2 protein and effectively reduce HK2 protein levels through lysosomal degradation (24).

In the present study, the targeting peptide TAT-ATXN1-CTM was used to degrade HK2 in an LPS-induced THP-1 cell model and murine ALI model. The results indicated that TAT-ATXN1-CTM may serve an anti-inflammatory role by degrading the HK2 protein. The present study provides a basis for novel treatment strategies for ALI via selective inhibition of glycolysis.

Materials and methods

Experimental animals. Adult male Institute of Cancer Research mice (n=72 animals, 6-8 weeks old, 25±2 g) were purchased from Shanghai Slack Experimental Animal Co., Ltd. [certificate no. SCXK (Hu) 2022-0004]. Mice were housed for 3 days to allow them to acclimate to the environment prior to the experiment. Mice were bred in specific pathogen-free conditions of 23±3˚C with 55±15% humidity and a 12 h light/dark cycle, and were allowed free access to sterilized food and water were supplied. All handling procedures used in the present study were approved by the Animal Care and Use Committees at the Zhejiang University School of Medicine (Approved No. ZJU20220294, Hangzhou, China) and were conducted in accordance with the policies of institutional guidelines on the care and use of laboratory animals. Euthanasia was performed with CO_2 at a volume displacement rate of 30% vol/min.

Murine model of ALI and treatment. Animals were divided into six groups in a randomized manner with 12 mice in each group. The groups were as follows: i) Control group; ii) LPS group; iii) LPS + TAT-CTM (200 μg/kg) group; iv) LPS + TAT-ATXN1-CTM (50 μg/kg) group; v) LPS + TAT-ATXN1-CTM (200 μg/kg) group; and vi) LPS + TAT-ATXN1-CTM (1,000 μg/kg) group. The mice were anesthetized by nasal inhalation of 4% isoflurane and the depth of anesthesia was maintained with 1.5% isoflurane. Mice in the control group were intratracheally injected with 0.9% sodium chloride injection (2 mg/kg). The murine ALI model was established by intratracheal injection of LPS (2 mg/kg; cat. no. L3129; MilliporeSigma). Treatment groups received LPS (2 mg/kg) and TAT-CTM (200 μg/kg) or TAT-ATXN1-CTM (50, 200, 1,000 μg/kg) administered simultaneously. Mice were euthanized once they reached humane endpoints or the study endpoint. The humane endpoints included signs of loose fur, inactivity or reduced activity, hunched posture, and respiratory distress, and these were not observed in any of the animals. The study endpoint was 8 h after LPS administration. The bronchoalveolar lavage fluid (BALF) was prepared to measure the accumulation of inflammatory cells, lung tissue was harvested for histopathological examination and the degree of pathological injury was scored.

Collection of BALF and cell counting. BALF preparation was described previously (25). Briefly, mice were sacrificed, and the trachea of each mouse was surgically exposed and cannulated. The left lung and accessory lobe were ligated to collect the BALF of the right lung. The right lung was lavaged twice with a single volume of warmed 0.5 ml of PBS containing 1% bovine serum albumin (cat. no. A8020; Beijing Solarbio) and 5,000 IU/l heparin. White blood cells were counted under a light microscope. The collected BALF was centrifuged at 400 x g, 4˚C for 10 min. The pelleted cells were coated onto microscope slides after drying at room temperature. Wright-Giemsa staining was performed, and the numbers of neutrophils, macrophages and lymphocytes were counted as cells/slide under a light microscope. Briefly, the slides were stained in Wright's stain (cat. no. W100940; Shanghai Aladdin Biochemical Technology Co., Ltd.) for 4 min and then in Giemsa's stain (cat. no. G100959; Shanghai Aladdin Biochemical Technology Co., Ltd.) for 2 min at 25˚C. The cells were observed and counted under the light microscope. Stained sections were scanned using the software Multiscan (2.0.0.150) of a digital section scanner (Convergence Technology Co., Ltd.) to obtain screenshots and analyze the processing. Neutrophils have a dark blue multi-lobed nucleus and pale pink cytoplasm; lymphocytes have purple nucleus

with sky blue cytoplasm; Macrophages have purple nucleus with blue cytoplasm as lymphocytes but larger than other leukocytes.

Histological examination of the lung. The left middle lobe of the lung was fixed in 10% neutral formalin overnight at room temperature and embedded in paraffin, and paraffin sections (5 μm) were prepared. The sections were stained with hematoxylin staining for 3 min and eosin staining for 30 sec at room temperature, and the lung injury and inflammatory cell infiltration were observed under a light microscope (26).

Inflammation score. The extent of histological lung damage was quantified by a designated scoring system, which is made up of five grades: 0 points, normal appearing lung; 1 point, mild inflammatory cell infiltration, no tissue injury; 2 points, mild to moderate inflammatory cell infiltration, mild tissue injury; 3 points, moderate inflammatory cell infiltration, mild tissue injury; 4 points, moderate to severe inflammatory cell infiltration with obvious tissue injury; and 5 points, severe inflammatory cell infiltration with significant tissue injury and changes. Slides were assessed by a pathologist blinded to the experimental design.

Cell culture. THP-1 and 293T cell lines were obtained from The Cell Bank of Type Culture Collection of The Chinese Academy of Sciences. The THP-1 human macrophages were cultured in RPMI-1640 growth medium (cat. no. CGM112.05; CellMax Technologies AB) containing 10% Premium FBS (cat. no. SA101.02; CellMax Technologies AB), 0.05 mM β-mercaptoethanol (cat. no. M6250; Shanghai Macklin Biochemical Co., Ltd.) and 1% penicillin-streptomycin. The 293T cells were cultured in DMEM (cat. no. CGM101.05; CellMax Technologies AB) with 10% FBS (cat. no. 04-001-1ACS; Biological Industries) and 1% penicillin-streptomycin. All cells were cultured in a CO_2 incubator at 37˚C with 5% CO_2. THP-1 cells ($5x10^5$ cells/ml) were treated with 100 ng/ml phorbol-12-myristate acetate (PMA; cat. no. HY-18739; MedChemExpress) for at 37˚C 24 h to induce cell attachment. The cells were further left to rest at 37˚C for 24 h in complete RPMI 1640 medium before stimulation with LPS (1 μg/ml; cat. no. L3129; MilliporeSigma) and 10 μM TAT-CTM or TAT-ATXN1-CTM treatments at 37˚C for 4, 8 and 24 h.

Cell transfection. The human HK2 plasmid containing the HK2 sequences and the pcDNA3.1 vector with three Flag tags were synthesized by Shandong Weizhen Biotechnology Co., Ltd. , and empty vector was used as a control. The 293T cells were plated on a 6-well plate to ~80% confluency 1 day before transfection, and then transfected with the plasmid. For transfection, 2 μg plasmid was diluted in 100 μl basal medium (DMEM) before adding to a 6-well plate. Polyethylenimine (PEI; cat. no. 23966; Polysciences, Inc.) at a 1:3 (w/w) cDNA:PEI ratio was added to the diluted plasmid solution and this was gently mixed. The plasmid-PEI mixture was placed in a CO_2 incubator for 20 min and then added to the cells, which were cultured in an incubator with 5% CO_2 at 37˚C. After 6 h, the solution in the 6-well plate was replaced with fresh complete medium, and 10 μM TAT-CTM or TAT-ATXN1-CTM (GenScript) for testing was added. Cells were harvested 48 h after transfection for subsequent experiments.

Table I. Amino acid sequences of ATXN1 (594-610), TAT, CTM, TAT-CTM and TAT-ATXN1-CTM.

Peptide	Amino acid sequence
ATXN1 (594-610)	KTEDFIQSAEISNDLKI
TAT	YGRKKRRQRR
CTM	KFERQKILDQRFFE
TAT-CTM	YGRKKRRQRRKFERQKILDQRFFE
TAT-ATXN1-CTM	YGRKKRRQRRKTEDFIQSAEISNDL KIKFERQKILDQRFFE

TAT, transactivator of transcription protein of HIV-1; ATXN1, ataxin 1; CTM, chaperone-mediated autophagy-targeting motif.

Cell viability assay. For MTT assays, $5x10^3$ THP-1 cells were seeded into 96-well plates with complete RPMI 1640 medium and treated with 100 ng/ml PMA at 37˚C for 24 h. The cells were further left to rest at 37˚C for 24 h in complete RPMI 1640 medium only before treatment with 0, 5, 10 and 20 μM of TAT-ATXN1-CTM or TAT-CTM in RPMI 1640 medium in a total volume of 100 μl at 37˚C for 24 h. Subsequently, 10 μl MTT/PBS (5 mg/ml; cat. no. M8180; Beijing Solarbio Science & Technology Co., Ltd.) was added to the medium and cells were incubated in a CO_2 incubator at 37˚C for 4 h. Subsequently, 100 μl dimethyl sulfoxide was added and the 96-well plates were shaken for 10 min at room temperature. Finally, optical density of the samples was measured at 490 nm using a multipurpose microplate reader (SpectraMax iD3; Molecular Devices, LLC).

Design, synthesis and testing of targeting peptide. It has been reported that the amino acid sequence 594-610 of ATXN1 interacts with the HK2 protein (24). To increase the membrane permeability of the peptide, a transmembrane domain (TAT) was added to the ATXN1 (594-610) sequence. A CTM sequence was added to degrade the endogenous targeted protein for lysosomal degradation (Table I).

TAT-ATXN1-CTM and TAT-CTM peptides, synthesized by GenScript, were solid-phase synthesized as C-terminal amides and purified using high-performance liquid chromatography (HPLC) using a preparative column, and the final purity was ascertained as 98.1% for TAT-ATXN1-CTM and 98.9% for TAT-CTM using analytical HPLC peak area integration (Figs. S1 and S2). Briefly, The TAT-ATXN1-CTM or TAT-CTM crude product was purified using an HPLC system (LC-20AB, Shimadzu) with the reversed-phase column (Inertsil ODS-3 4.6x250 mm, Shimadzu) at 25 ˚C. The samples were loaded onto the column (12-15 μl loading volume). The flow rate was set to be 1 ml/min using 0.065% trifluoroacetic in 100% water (v/v) and 0.05% trifluoroacetic in 100% acetonitrile (v/v) as the mobile phase compositions of pump A and pump B, respectively. The wavelength of the detector was set to 220 nm. The purified TAT-ATXN1-CTM or TAT-CTM fractions were collected. The molecular masses of the peptides

were determined by electrospray ionization mass spectrometry (ESI-MS, LCMS-2020, Shimadzu). MS parameters for the peptides were: nitrogen gas temperature, 350˚C; gas flow, 5 l/min; nebulizer pressure, 15 psi; scan time, 500 msec. The observed mass spectral values for TAT-ATXN1-CTM and TAT-CTM were 5,359.2 and 3,270.0, respectively, which was consistent with the theoretical values (Figs. S3 and S4).

Reverse transcription-quantitative PCR (RT-qPCR). Total RNA was extracted from cells using TRIzol® reagent (cat. no. CW0580S; CoWin Biosciences) according to the manufacturer's instructions. Total RNA was quantified using a micro-spectrophotometer (NAno-300; cat. no. MO00040009; Hangzhou Allsheng Instruments Co., Ltd.), and the optical density 260/280 nm ratio of all samples was 1.8-2.0. Next, cDNA was synthesized on a PCR instrument (SimpliAmp™; cat. no. A24811; Thermo Fisher Scientific, Inc.) using the RNA reverse transcription kit (cat. no. CW2569M; CoWin Biosciences). RT was performed as follows: 42˚C for 15 min, incubate at 85˚C for 5 min, and keep warm at 4˚C. Primers and a fluorescent quantitative PCR kit (cat. no. CW2601H; CoWin Biosciences) containing SYBR Green I fluorescent dye were used to perform fluorescent qPCR on a PCR system (cat. no. 4351106; Thermo Fisher Scientific, Inc.). Primer sequences for human HK2, human GAPDH, mouse HK2 and mouse β-actin (Sangon Biotech Co., Ltd.) are listed in Table II. The thermocycling conditions were as follows: 95˚C for 10 min, followed by 40 cycles of 95˚C for 15 sec and 60˚C for 60 sec. The $2^{-\Delta\Delta Cq}$ method was used for analysis of results and gene levels were normalized to the internal reference gene, GAPDH for human HK2 or β-actin for mouse HK2 (27).

Western blotting. The cells were washed with pre-cooled 1X PBS (cat. no. P1020; Beijing Solarbio Science & Technology Co., Ltd.) and lysed with lysis buffer containing RIPA (cat. no. P0013B; Beyotime Institute of Biotechnology) and PMSF (cat. no. P0100; Beijing Solarbio Science & Technology Co., Ltd.) at a ratio of 1:100 of PMSF:RIPA. The cell lysate was centrifuged at 13,800 x g for 5 min at 4˚C to obtain the supernatant. The protein content of the supernatant was determined using a BCA Protein Assay Kit (cat. no. BL521A; Biosharp Life Sciences) and then protein (20 μg/lane) were loaded onto 10% sodium dodecyl sulfate-polyacrylamide gel electrophoresis before being electrophoretically transferred onto PVDF membranes (cat. no. 1214429; GVS). The membrane was blocked with ready-to-use blocking solution (cat. no. P0252; Beyotime Institute of Biotechnology) for 1 h at room temperature and then incubated with the indicated primary antibodies overnight at 4˚C. The primary antibodies were as follows: Anti-β-actin (1:1,000; cat. no. 3700; Cell Signaling Technology, Inc.), anti-HK1 (1:1,000; cat. no. 2024S; Cell Signaling Technology, Inc.) and anti-HK2 (1:1,000; cat. no. ab209874; Abcam). Subsequently, the following secondary antibodies were added for 1 h at room temperature: Goat anti-rabbit IgG HRP-conjugated (1:12,000; cat. no. 31460; Thermo Fisher Scientific, Inc.) and goat anti-mouse IgG HRP-conjugated (1:12,000; cat. no. 31430; Thermo Fisher Scientific, Inc.). Detection of immunoreactive bands was performed using ECL Western Blotting Detection kit (cat. no. SW2040; Beijing Solarbio Science & Technology Co., Ltd.) on a chemiluminescence gel imaging system (Peiqing JS-1070P; Shanghai Peiqing Science & Technology Co., Ltd.) and data were semi-quantified using ImageJ2x 2.1.4.7 (Rawak Software Development) with β-actin as the loading control.

Table II. Primer sequences.

Gene	Primer	Sequence (5'-3')
Human HK2	Forward	TTGACCAGGAGATTGACATGGG
	Reverse	CAACCGCATCAGGACCTCA
Human GAPDH	Forward	GGAGCGAGATCCCTCCAAAAT
	Reverse	GGCTGTTGTCATACTTCTCATGG
Mouse HK2	Forward	GTGTGCTCCGAGTAAGGGTG
	Reverse	CAGGCATTCGGCAATGTGG
Mouse β-actin	Forward	GGCTGTATTCCCCTCCATCG
	Reverse	CCAGTTGGTAACAATGCCATGT

HK2, hexokinase 2.

ELISA. The lung tissues from mice and supernatants from THP-1 cells were collected. For lung tissues, the protein concentration was assayed using a BCA Protein Assay Kit (cat. no. BL521A; Biosharp Life Sciences). Levels of TNF-α, IL-1β and HK2 were analyzed using commercial ELISA kits according to the manufacturer's instructions. Human TNF-α ELISA Kit (cat. no. CHE0019; Beijing 4A Biotech Co., Ltd.), Human IL-1β ELISA Kit (cat. no. CHE0001; Beijing 4A Biotech Co., Ltd.), Mouse TNF-α ELISA Kit (cat. no. CME0004; Beijing 4A Biotech Co., Ltd.), Mouse IL-1β (cat. no. CME0015; Beijing 4A Biotech Co., Ltd.) and Mouse HK2 ELISA kit (cat. no. ml058727; Mlbio) were used. The absorbance of each well was measured at 450 nm with a multifunctional microplate reader (SpectraMax iD3; Molecular Devices, LLC), and the concentration of TNF-α, IL-1β and HK2 was calculated according to the standard curve.

Statistical analysis. Statistical analyses were performed using GraphPad Prism 7.0 (Dotmatics). All quantitative results are presented as the mean ± standard error of the mean (SEM) from at least three independent experiments. Statistical analysis was performed using one-way ANOVA followed by Dunnett's post hoc test, two-way ANOVA followed by Sidak's post hoc test, Kruskal-Wallis test followed by Dunn's post hoc test or an unpaired two-tailed Student's t-test. $P<0.05$ was considered to indicate a statistically significant difference.

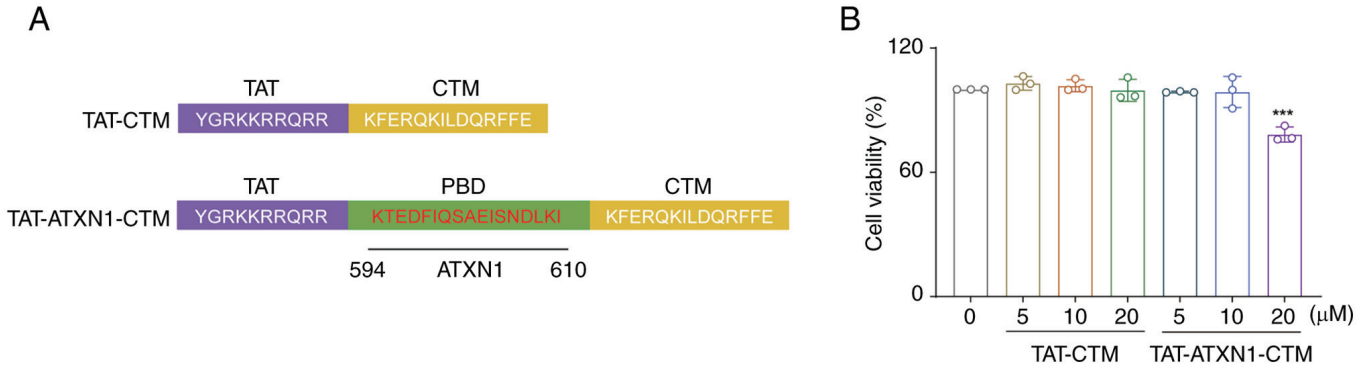

Figure 1. Composition and safety profile of TAT-ATXN1-CTM. (A) Structural diagrams of TAT-ATXN1-CTM and nonfunctional peptide TAT-CTM. TAT-ATXN1-CTM consists of three functional domains, including TAT, PBD and CTM. (B) Effects of TAT-ATXN1-CTM on the viability of THP-1 cells assessed using an MTT assay. THP-1 cells were treated with different concentrations (0, 5, 10 and 20 μM) of TAT-ATXN1-CTM or TAT-CTM for 24 h. Data are presented as the mean ± SEM (n=3). One-way ANOVA followed by Dunnett's post hoc test was used to assess significance. ***P<0.001 vs. 0 μM. TAT, transactivator of transcription protein of HIV-1; ATXN1, ataxin 1; CTM, chaperone-mediated autophagy-targeting motif; PBD, protein-binding domain.

Results

Composition and safety assessment of TAT-ATXN1-CTM in vitro. TAT-ATXN1-CTM was designed to cross the cell membrane and selectively degrade the HK2 protein. The peptide consists of three functional domains. The first domain (TAT) can induce the peptide to cross the cell membrane. The second domain (PBD) is composed of ATXN1 protein, which can selectively recognize and bind to the HK2 protein. The third domain, CTM, targets lysosomes to degrade proteins (23,24). In the present study, TAT-CTM was used as a control (Fig. 1A).

The effects of TAT-ATXN1-CTM at different concentrations on cell viability were assessed using an MTT assay. The results demonstrated that TAT-ATXN1-CTM treatment for 24 h at 5 and 10 μM had no significant effects on the viability of THP-1 cells, while 20 μM treatment significantly decreased the cell viability compared with the 0 μM treated group [Fig. 1B; 20 μM (TAT-ATXN1-CTM) vs. 0 μM, 78.290±2.099 vs. 100.000±0.000; P<0.001]. Therefore, 10 μM TAT-ATXN1-CTM was used for subsequent experiments to avoid cytotoxicity (Fig. 1B).

TAT-ATXN1-CTM selectively degrades HK2 protein without changing HK2 mRNA levels in vitro. Firstly, HK2 was overexpressed and it was confirmed by both western blotting and RT-qPCR that HK2 expression was increased following transfection with the HK2 plasmid compared with the empty vector group (Fig. S5, HK2 plasmid vs. empty vector, for mRNA, 8.257±0.905 vs. 1.016±0.121, P<0.01; Fig. 2A, for protein, 2.955±0.148 vs. 1.000, P<0.001). Subsequently, the degradation of the HK2 protein by TAT-ATXN1-CTM was verified. TAT-ATXN1-CTM treatment significantly reduced HK2 expression following HK2 plasmid-mediated overexpression in 293T cells (Fig. 2A; HK2 plasmid$^+$/TAT-ATXN1-CTM$^+$ vs. HK2 plasmid$^+$, 2.003±0.106 vs. 2.955±0.148; P<0.001). In LPS-induced THP-1 cells, TAT-ATXN1-CTM treatment also markedly reduced HK2 protein expression [Fig. 2B; LPS$^+$/control$^+$ vs. vehicle (Veh)$^+$/control$^+$, 1.826±0.076 vs. 1.000; P<0.001; LPS$^+$/TAT-ATXN1-CTM$^+$ vs. LPS$^+$/control$^+$, 1.196±0.096 vs. 1.826±0.076; P<0.01]. By contrast, HK2 mRNA levels were significantly increased at 4 and 8 h after LPS treatment, but were not affected at different time points (4, 8 and 24 h) after TAT-ATXN1-CTM administration (Fig. 2C; LPS vs. control, 4 h: 3.611±0.1444 vs. 1.003±0.0561, P<0.05, 8 h: 5.601±0.5804 vs. 0.973±0.0214, P<0.001). In addition, TAT-ATXN1-CTM treatment tended to decrease HK1 protein expression in LPS-induced THP-1 cells (Fig. 2B; LPS$^+$/TAT-ATXN1-CTM$^+$ vs. LPS$^+$/control$^+$, 0.717±0.0417 vs. 0.939±0.060; P=0.141), possibly through indirect mechanisms related to inflammation suppression. These results suggested that TAT-ATXN1-CTM was effective in selectively reducing HK2 expression.

TAT-ATXN1-CTM reduces the production of proinflammatory factors in LPS-induced THP-1 cells. HK2 expression is increased during inflammatory processes (28) and whether TAT-ATXN1-CTM exerted anti-inflammatory effects by degrading the HK2 protein was next investigated. Treatment with 10 μM TAT-ATXN1-CTM significantly reduced the levels of TNF-α and IL-1β in the supernatant of THP-1 cells induced by LPS (Fig. 3; LPS$^+$/control$^+$ vs. Veh$^+$/control$^+$, TNF-α: 25.670±1.015 vs. 0.194±0.009, P<0.001, IL-1β: 12.840±0.699 vs. 0.637±0.0554, P<0.001; LPS$^+$/TAT-ATXN1-CTM$^+$ vs. LPS$^+$/control$^+$, TNF-α: 17.860±0.184 vs. 25.670±1.015, P<0.001, IL-1β: 8.739±0.291 vs. 12.840±0.699, P<0.001). Notably, TAT-CTM, as a control treatment, also decreased IL-1β protein expression (Fig. 3B; LPS$^+$/TAT-CTM$^+$ vs. LPS$^+$/control$^+$, IL-1β: 9.458±0.425 vs. 12.840±0.699; P<0.001). These data imply that TAT-ATXN1-CTM could suppress proinflammatory cytokines in LPS-induced THP-1 cells.

TAT-ATXN1-CTM attenuates inflammatory cell infiltration in the lung in an LPS-induced model of ALI. The anti-inflammatory effect of TAT-ATXN1-CTM was investigated in a murine model of ALI (Fig. 4A). TAT-ATXN1-CTM (1,000 μg/kg) treatment significantly reduced the number of total cells, neutrophils, macrophages and lymphocytes in the BALF compared to the control group [Fig. 4B-F; LPS$^+$ vs. control, total cells: 47.050±3.004 vs. 9.545±0.796, P<0.001, neutrophils: 15.900±2.424 vs. 0.05±0.017, P<0.001, macrophages: 5.330±1.396 vs. 0.036±0.010, P<0.001 and

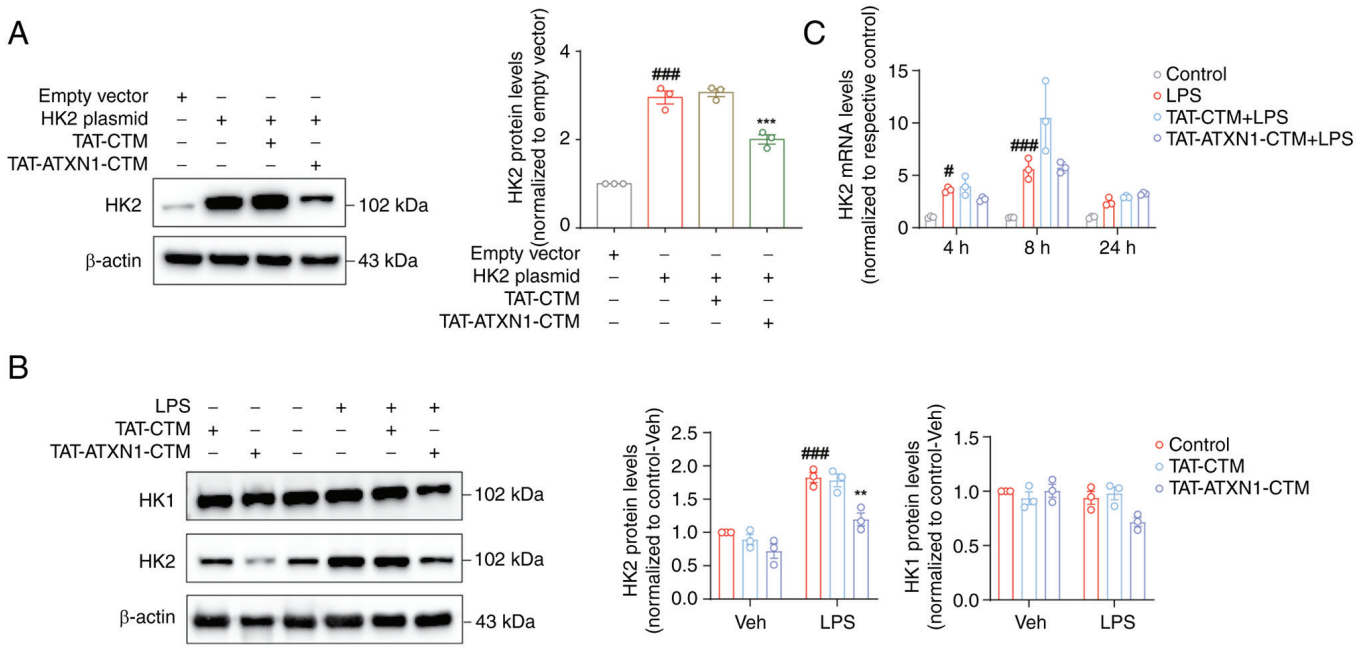

Figure 2. TAT-ATXN1-CTM selectively degrades HK2 protein without affecting its mRNA level. (A) Representative immunoblots and semi-quantification demonstrated that TAT-ATXN1-CTM at 10 μM reduced HK2 protein expression in HK2-overexpressing 293T cells. One-way ANOVA followed by Dunnett's post hoc test was used to assess significance. $^{###}$P<0.001 vs. empty vector; ***P<0.001 vs. HK2 plasmid^{+}. (B) Representative immunoblots and semi-quantification demonstrated that TAT-ATXN1-CTM (10 μM) reduced the LPS-induced elevated protein expression of HK2 in THP-1 cells. (C) TAT-ATXN1-CTM (10 μM) had no effects on the LPS-induced elevated mRNA levels of HK2 in cells at 4, 8 and 24 h. Data are presented as the mean ± SEM (n=3). Two-way ANOVA followed by Sidak's post hoc test was used to assess significance. $^{#}$P<0.05, $^{###}$P<0.001 vs. respective control; **P<0.01 vs. LPS^{+}/control^{+}. TAT, transactivator of transcription protein of HIV-1; ATXN1, ataxin 1; CTM, chaperone-mediated autophagy-targeting motif; HK, hexokinase; LPS, lipopolysaccharide; Veh, vehicle.

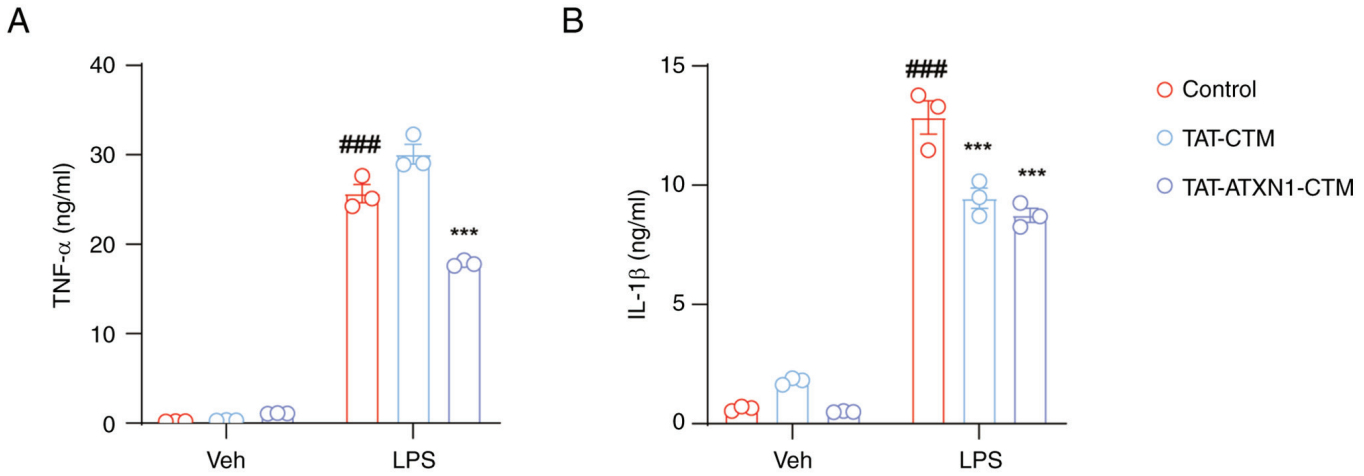

Figure 3. TAT-ATXN1-CTM reduces the LPS-induced production of inflammatory factors. TAT-ATXN1-CTM (10 μM) significantly attenuated the LPS-induced elevated protein levels of (A) TNF-α and (B) IL-1β in the supernatant. Data are presented as the mean ± SEM (n=3). Two-way ANOVA followed by Sidak's post hoc test was used to assess significance. $^{###}$P<0.001 vs. respective control; ***P<0.001 vs. LPS^{+}/control^{+}. TAT, transactivator of transcription protein of HIV-1; ATXN1, ataxin 1; CTM, chaperone-mediated autophagy-targeting motif; LPS, lipopolysaccharide; Veh, vehicle.

lymphocytes: 25.820±2.746 vs. 9.460±0.784, P<0.001; LPS^{+}/TAT-ATXN1-CTM (1,000 μg/kg)$^{+}$ vs. LPS^{+}, total cells: 20.000±1.676 vs. 47.050±3.004, P<0.001, neutrophils: 5.985±1.044 vs. 15.900±2.424, P<0.01, macrophages: 1.570±0.227 vs. 5.330±1.396, P<0.001 and lymphocytes: 12.450±1.303 vs. 25.820±2.746, P<0.001]. Notably, TAT-CTM also slightly decreased the number of total cells (Fig. 4C; total cells: 36.130±2.010 vs. 47.050±3.004; P<0.01), macrophages (Fig. 4E; 2.560±0.392 vs. 5.330±1.396; P<0.05) and lymphocytes (Fig. 4F; 18.220±1.655 vs. 25.820±2.746; P<0.01) in BALF. In conclusion, these data suggested that TAT-ATXN1-CTM treatment inhibited the accumulation of inflammatory cells in the lungs of LPS-induced mice.

TAT-ATXN1-CTM attenuates pathological injury in the lungs in an LPS-induced model of ALI. Based on lung histological examination, LPS induced a pulmonary inflammatory response, including notable alveolar wall

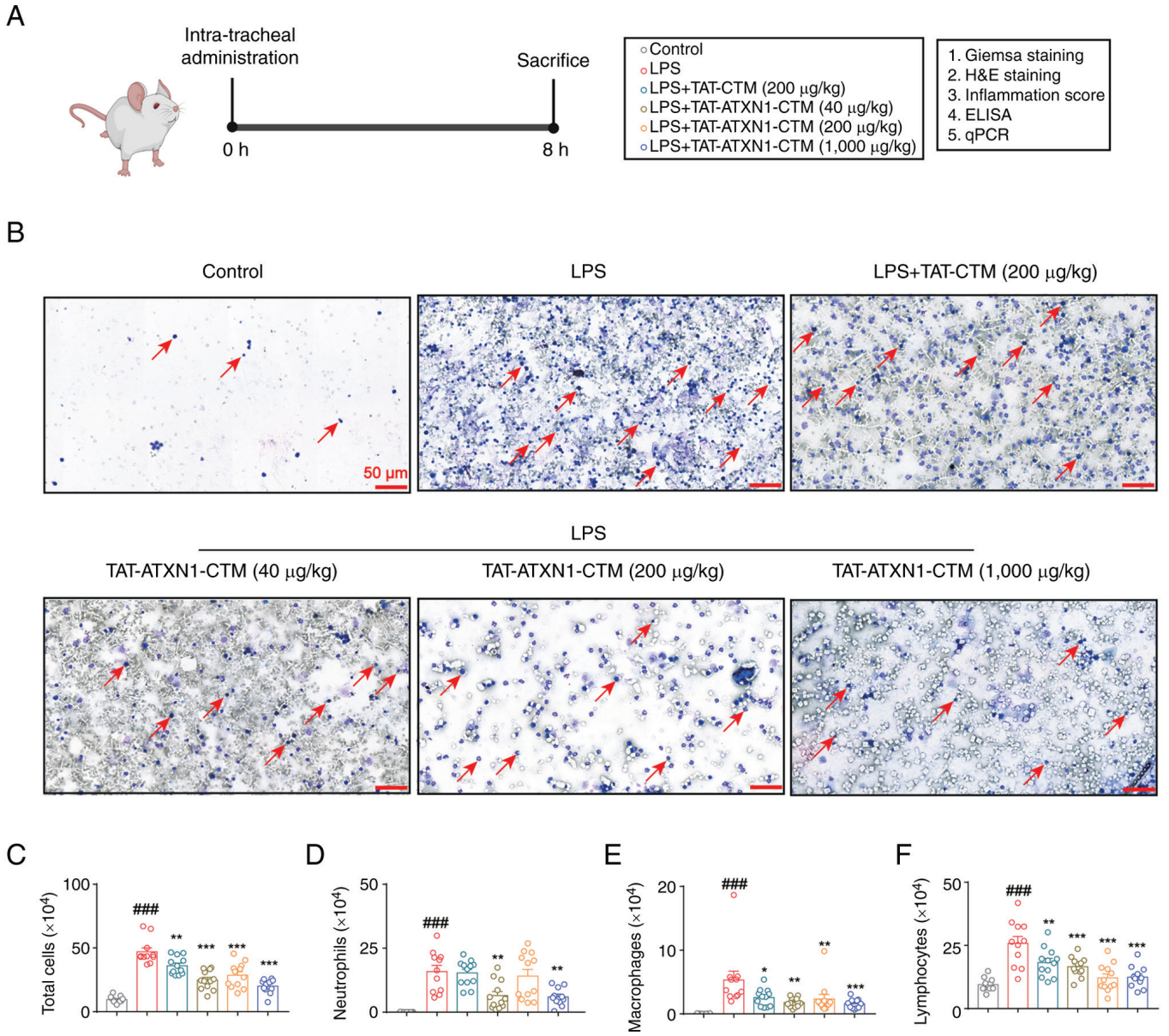

Figure 4. TAT-ATXN1-CTM treatment reduces the accumulation of inflammatory cells in LPS-induced mice. (A) Schematic representation of the protocol used for the mouse experiments. (B) Representative images of Wright-Giemsa staining of the BALF cells are shown. Scale bar, 50 μm. The arrows point to white blood cells. (C) Total cells, (D) neutrophils, (E) macrophages and (F) lymphocytes in the BALF were counted. Data are presented as the mean ± SEM (n=11-12). One-way ANOVA followed by Dunnett's post hoc test was used to assess significance. $^{###}$P<0.001 vs. control; *P<0.05, **P<0.01, ***P<0.001 vs. LPS^{+}. TAT, transactivator of transcription protein of HIV-1; ATXN1, ataxin 1; BALF, bronchoalveolar lavage fluid; CTM, chaperone-mediated autophagy-targeting motif; LPS, lipopolysaccharide; qPCR, quantitative PCR.

thickening, congestion with inflammatory cell infiltration around the alveoli or airways, which was significantly attenuated by 1,000 μg/kg TAT-ATXN1-CTM treatment [Fig. 5; LPS^{+} vs. control, 2.727±0.333 vs. 0.083±0.083, P<0.001; LPS^{+}/TAT-ATXN1-CTM (1,000 μg/kg)$^{+}$ vs. LPS^{+}, 1.364±0.152 vs. 2.727±0.333, P<0.05]. These results indicated that inhibition of HK2 attenuated lung histopathological damage in LPS-induced ALI in mice.

TAT-ATXN1-CTM treatment suppresses HK2 protein expression and proinflammatory factors in the lungs of LPS-treated mice. Based on the aforementioned findings, TAT-ATXN1-CTM (1,000 μg/kg) ameliorated ALI *in vivo*, whereas other low concentrations of TAT-ATXN1-CTM had limited effect in treating ALI. Consequently, the effects of TAT-ATXN1-CTM (1,000 μg/kg) on the expression of HK2 and proinflammatory factors in LPS-challenged mice only were investigated. TAT-ATXN1-CTM (1,000 μg/kg) treatment reduced the protein expression levels of HK2, TNF-α and IL-1β without affecting HK2 mRNA levels in the lung tissues of ALI mice [Fig. 6; LPS^{+} vs. control, HK2: 0.744±0.045 vs. 0.320±0.004, P<0.001, TNF-α: 420.600±32.250 vs. 158.800±4.788, P<0.001 and IL-1β: 129.300±12.040 vs. 17.630±0.921, P<0.001; LPS^{+}/TAT-ATXN1-CTM^{+} (1,000 μg/kg) vs. LPS^{+}, HK2: 0.461±0.021 vs. 0.744±0.045, P<0.001, TNF-α: 262.500±15.750 vs. 420.600±32.250, P<0.001 and IL-1β: 59.040±5.229 vs. 129.300±12.040, P<0.001]. Collectively, these data suggested that 1,000 μg/kg

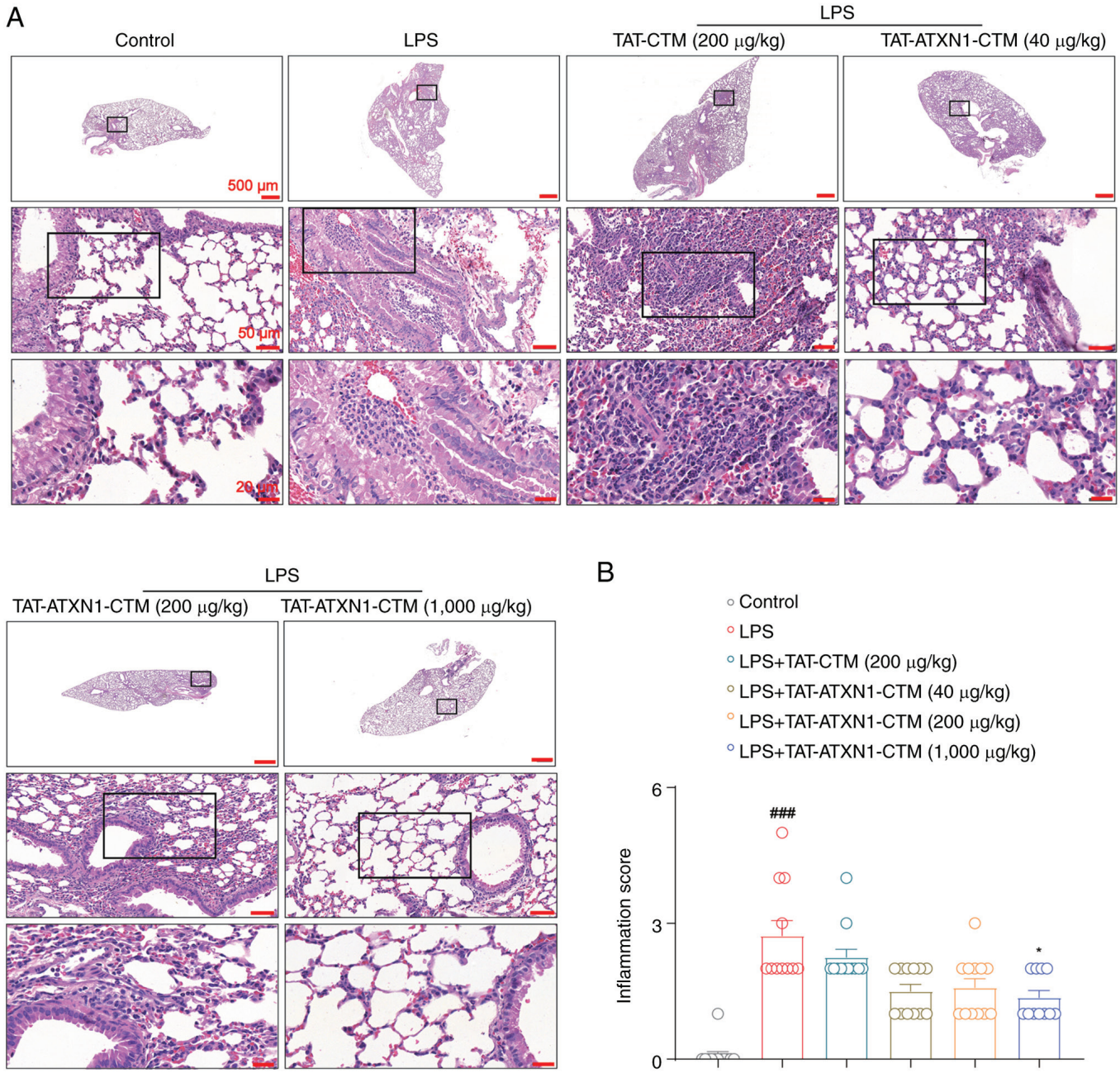

Figure 5. TAT-ATXN1-CTM attenuates pathological injury in the lung tissues of LPS-induced mice. (A) Lung histopathology of mice (H&E staining). Scale bar, 500 μm (top row), 50 μm (middle row) or 20 μm (bottom row). (B) Inflammation score of lung histology. Data are presented as the mean ± SEM (n=11-12). Kruskal-Wallis test followed by Dunn's post hoc test was used to assess significance. $^{###}$P<0.001 vs. control; *P<0.05 vs. LPS^{+}. TAT, transactivator of transcription protein of HIV-1; ATXN1, ataxin 1; CTM, chaperone-mediated autophagy-targeting motif; LPS, lipopolysaccharide.

TAT-ATXN1-CTM reduced the protein expression levels of HK2 and proinflammatory factors in ALI mice induced by LPS.

Discussion

ALI is a devastating intrapulmonary inflammatory disease and there is a lack of effective drug treatments (9). In the present study, a peptide, TAT-ATXN1-CTM, was designed, and this could enter cells using TAT, bind to the HK2 protein via the PBD and transport the peptide-HK2 protein complex to the lysosome for degradation via CTM, which alleviates LPS-induced ALI (Fig. 7). The present study provided experimental evidence that TAT-ATXN1-CTM exerted anti-inflammatory effects through HK2 degradation in the treatment of ALI. However, the THP-1 and 293T cells used in the experiments were immortalized tumor cells, and validation using primary macrophages from humans is needed. In addition, while TAT-ATXN1-CTM exerted potent anti-inflammatory activity *in vitro*, it had relatively minor efficacy *in vivo* and higher drug concentrations are required to protect mice from LPS-induced ALI, which may be related to factors such as the shorter half-life and lower stability of the peptide (29). Therefore, TAT-ATXN1-CTM needs to be further optimized or modified to improve its stability and potency via the introduction of stabilizing α-helixes, salt

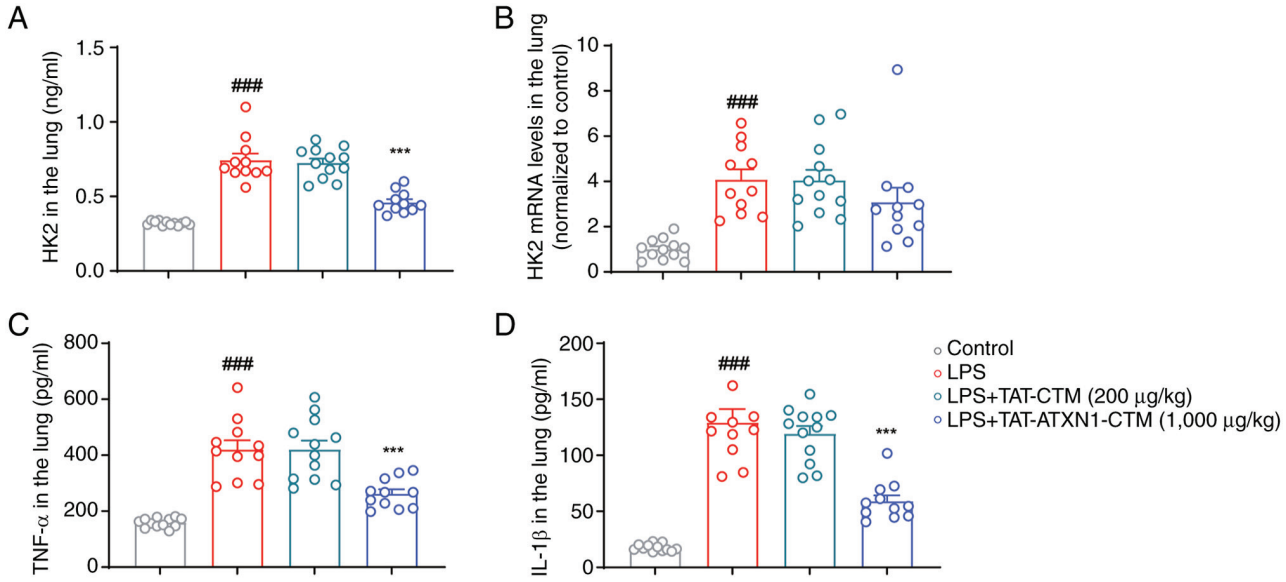

Figure 6. TAT-ATXN1-CTM treatment decreases the protein expression of HK2 and pro-inflammatory factors in the lungs of LPS-treated mice. TAT-ATXN1-CTM (1,000 μg/kg) significantly attenuated the LPS-induced elevated protein levels of (A) HK2, (C) TNF-α and (D) IL-1β, without influencing (B) HK2 mRNA expression in the lung tissues. Data are presented as the mean ± SEM (n=11-12). One-way ANOVA followed by Dunnett's post hoc test was used to assess significance. $^{###}$P<0.001 vs. control; ***P<0.001 vs. LPS group. TAT, transactivator of transcription protein of HIV-1; ATXN1, ataxin 1; CTM, chaperone-mediated autophagy-targeting motif; HK2, hexokinase 2; LPS, lipopolysaccharide.

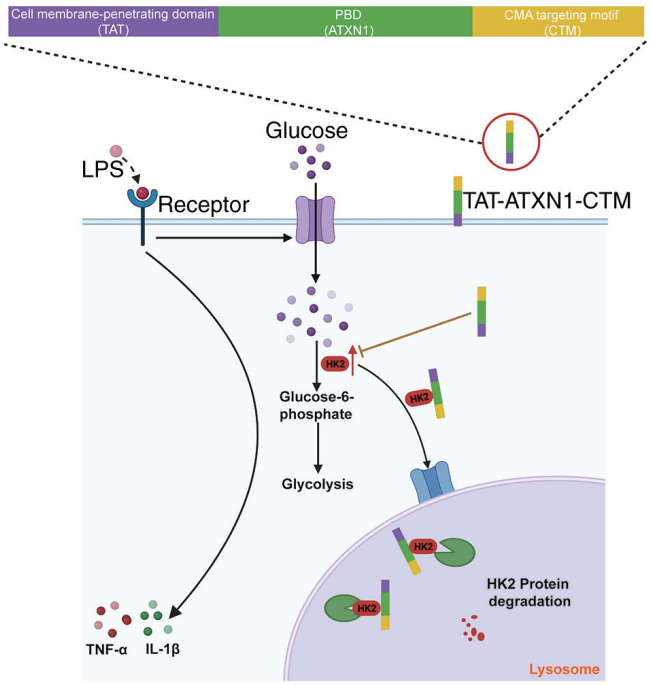

Figure 7. TAT-ATXN1-CTM attenuates LPS-induced ALI by mediating HK2 protein degradation. TAT-ATXN1-CTM enters the cell through its cell membrane-penetrating domain (TAT), binds to the HK2 protein via the PBD and chaperones the degrading peptide-HK2 protein complex to the lysosome for degradation via its CTM, alleviating the LPS-induced ALI. ALI, acute lung injury; TAT, transactivator of transcription protein of HIV-1; ATXN1, ataxin 1; CTM, chaperone-mediated autophagy-targeting motif; HK2, hexokinase 2; LPS, lipopolysaccharide; PBD, protein-binding domain.

bridge formations, stapling or clipping of peptide sequences, or other chemical modifications in future studies (29). Furthermore, an optimal dose needs to be determined based on numerous factors, including the bioavailability, pharmacokinetics and toxicity of the peptide, which requires further characterization.

To date, there are two main ways to silence proteins. RNA interference (RNAi) technology is the more commonly used approach for protein expression knockdown due to its relative maturity in terms of precision and efficacy (30). However, this technology presents some experimental side effects, such as prolonged duration of action, suppression of genes other than the desired gene target, resulting in impeding other non-target protein expression and disrupting the natural regulatory mechanism of normal cells (31). Additionally, the introduction of exogenous RNA can stimulate the production of inflammatory factors and cause cell damage (32). Furthermore, the clustered regularly interspaced short palindromic repeat-associated protein 9 (Cas9) system is a highly efficient genome editing method that allows for precise modification of genomic DNA to interfere with the expression of specific proteins (33). Compared with RNAi technology, gene knockout has demonstrated superior consistency (34). However, it still faces challenges in terms of delivery, specificity, toxicity and immune responses. For example, Cas9 can be delivered in the forms of DNA, mRNA, or protein. Plasmid DNA poses a risk of insertional mutagenesis (35); delivering the Cas9 protein, which is of bacterial origin, into cells may induce carryover of bacterial endotoxin and trigger serious immunologic responses (36); the cell-targeting specificity of Cas9 delivery requires novel biomaterials to address (37).

The method used in the present study has some superiority over other methods for targeting peptides. The peptide is easy and inexpensive to prepare, with specificity being its most crucial characteristic. The specificity and effectiveness of targeting peptides to degrade specific proteins largely depend on the affinity and high selectivity of the interaction between target proteins and PBDs (23). Common methods for the identification of high-affinity and specific PBDs include peptide

arrays, phage display and computational modeling (23,38). A sequence based on the binding site between the HK2 and ATXN1 proteins was designed. We hypothesized that ATXN1 has a specific motif for binding to HK2, and the binding relationship between ATXN1 and HK2 was simulated. It was found that ATXN1 (594-610) interacted with HK2, and thus, the ATXN1 (594-610) sequence was used for the PBD.

Emerging evidence has indicated reciprocal regulation between glucose metabolism and immunity (39). Increased glycolysis facilitated by pyruvate kinase M2 contributes substrates for the biosynthesis of proteins and nucleic acids needed for LPS-induced inflammatory activation of immune cells (39,40). Furthermore, previous studies have demonstrated that HK2 protein was an important regulatory factor in the regulation of inflammation-related diseases, and HK2 protein silencing could inhibit the production of inflammatory factors (41,42). In the present study, it was verified that TAT-ATXN1-CTM degraded HK2 protein without affecting its mRNA levels both *in vitro* and *in vivo*, which was consistent with the results of a previous study (23). Under normal conditions, TAT-ATXN1-CTM had no effect on the HK1 protein; however, in THP-1 cell inflammatory models, it tended to downregulate HK1 protein expression. This may be related to the reduced inflammatory response resulting from HK2 degradation, which can result in decreased HK1 expression (12). Furthermore, the degradation of HK2 may induce increased G-6P levels, and then upregulated cellular glucose uptake, which may in turn inhibit HK1 (12,43). In addition, the TAT-CTM control reduced levels of the inflammatory factor IL-1β and decreased inflammatory leukocyte production. It has been reported that increased expression and activation of NLRP3 inflammasome protein components promoted IL-1β production and recruitment of immune cells to the site of injury, and NLRP3 proteins are considered to be substrates for CMA (44,45). Therefore, we hypothesized that TAT-CTM containing the CMA structure may reduce IL-1β production and inflammatory cell infiltration by promoting NLRP3 protein degradation.

In conclusion, the present study demonstrated that the TAT-ATXN1-CTM targeting peptide could effectively degrade the endogenous HK2 protein and act as an anti-inflammatory agent *in vitro* and *in vivo*. Therefore, the outcome of the experiments provides novel perspectives for TAT-ATXN1-CTM application in the development of ALI treatment, and provides novel insights for drug discovery. Finally, it is hypothesized that targeting peptides hold great potential as an effective therapeutic approach in the future, as shown by a successful phase 2B clinical trial, which elucidated the efficacy and safety of TAT-mediated peptides (46).

Acknowledgements

Not applicable.

Funding

The present study was supported by grants from The National Natural Science Foundation of China (grant no. 82173819) and Natural Science Foundation of Zhejiang Province (grant no. LTGY23H010006).

Availability of data and materials

The data generated in the present study may be requested from the corresponding author.

Authors' contributions

YX and HG conceived and designed the study. JY, LD and YW performed the experiments and analyzed the results. JY and YX wrote and revised the manuscript. LD, LG and YW participated in the data analysis and interpretation. YX and JY confirm the authenticity of all the raw data. All authors read and approved the final version of the manuscript.

Ethics approval and consent to participate

All handling procedures used in the present study were approved by the Animal Care and Use Committees at the Zhejiang University School of Medicine (Approved No. ZJU20220294, Hangzhou, China) and were conducted in accordance with the policies of institutional guidelines on the care and use of laboratory animals.

Patient consent for publication

Not applicable.

Competing interests

The authors declare that they have no competing interests.

References

1. Jiang R, Xu J, Zhang Y, Zhu X, Liu J and Tan Y: Ligustrazine alleviate acute lung injury through suppressing pyroptosis and apoptosis of alveolar macrophages. Front Pharmacol 12: 680512, 2021.
2. Mowery NT, Terzian WTH and Nelson AC: Acute lung injury. Curr Probl Surg 57: 100777, 2020.
3. Dutta S, Zhu Y, Han Y, Almuntashiri S, Wang X and Zhang D: Long Noncoding RNA: A novel insight into the pathogenesis of acute lung injury. J Clin Med 12: 604, 2023.
4. He YQ, Zhou CC, Yu LY, Wang L, Deng JL, Tao YL, Zhang F and Chen WS: Natural product derived phytochemicals in managing acute lung injury by multiple mechanisms. Pharmacol Res 163: 105224, 2021.
5. Qian J, Chen X, Shu S, Zhang W, Fang B, Chen X, Zhao Y, Liu Z and Liang G: Design and synthesis novel di-carbonyl analogs of curcumin (DACs) act as potent anti-inflammatory agents against LPS-induced acute lung injury (ALI). Eur J Med Chem 167: 414-425, 2019.
6. Yuan R, Li Y, Han S, Chen X, Chen J, He J, Gao H, Yang Y, Yang S and Yang Y: Fe-curcumin nanozyme-mediated reactive oxygen species scavenging and Anti-Inflammation for acute lung injury. ACS Cent Sci 8: 10-21, 2022.
7. Goodman RB, Pugin J, Lee JS and Matthay MA: Cytokine-mediated inflammation in acute lung injury. Cytokine Growth Factor Rev 14: 523-535, 2003.
8. Johnston LK, Rims CR, Gill SE, McGuire JK and Manicone AM: Pulmonary macrophage subpopulations in the induction and resolution of acute lung injury. Am J Respir Cell Mol Biol 47: 417-426, 2012.
9. Zhong WJ, Yang HH, Guan XX, Xiong JB, Sun CC, Zhang CY, Luo XQ, Zhang YF, Zhang J, Duan JX, *et al*: Inhibition of glycolysis alleviates lipopolysaccharide-induced acute lung injury in a mouse model. J Cell Physiol 234: 4641-4654, 2018.
10. Rodriguez-Prados JC, Traves PG, Cuenca J, Rico D, Aragonés J, Martín-Sanz P, Cascante M and Boscá L: Substrate fate in activated macrophages: A comparison between innate, classic, and alternative activation. J Immunol 185: 605-614, 2010.

11. Zhong WJ, Liu T, Yang HH, Duan JX, Yang JT, Guan XX, Xiong JB, Zhang YF, Zhang CY, Zhou Y and Guan CX: TREM-1 governs NLRP3 inflammasome activation of macrophages by firing up glycolysis in acute lung injury. Int J Biol Sci 19: 242-257, 2023.
12. Roberts DJ and Miyamoto S: Hexokinase II integrates energy metabolism and cellular protection: Akting on mitochondria and TORCing to autophagy. Cell Death Differ 22: 248-257, 2015.
13. DeWaal D, Nogueira V, Terry AR, Patra KC, Jeon SM, Guzman G, Au J, Long CP, Antoniewicz MR and Hay N: Hexokinase-2 depletion inhibits glycolysis and induces oxidative phosphorylation in hepatocellular carcinoma and sensitizes to metformin. Nat Commun 9: 446, 2018.
14. Gong L, Cui Z, Chen P, Han H, Peng J and Leng X: Reduced survival of patients with hepatocellular carcinoma expressing hexokinase II. Med Oncol 29: 909-914, 2012.
15. Hu Y, Cao K, Wang F, Wu W, Mai W, Qiu L, Luo Y, Ge WP, Sun B, Shi L, *et al*: Dual roles of hexokinase 2 in shaping microglial function by gating glycolytic flux and mitochondrial activity. Nat Metab 4: 1756-1774, 2022.
16. Varghese E, Samuel SM, Líšková A, Samec M, Kubatka P and Büsselberg D: Targeting glucose metabolism to overcome resistance to anticancer chemotherapy in breast cancer. Cancers (Basel) 12: 2252, 2020.
17. Chen CH, Wang BW, Hsiao YC, Wu CY, Cheng FJ, Hsia TC, Chen CY, Wang Y, Weihua Z, Chou RH, T, *et al*: PKCdelta-mediated SGLT1 upregulation confers the acquired resistance of NSCLC to EGFR TKIs. Oncogene 40: 4796-4808, 2021.
18. Ros S and Schulze A: Glycolysis back in the limelight: Systemic targeting of HK2 blocks tumor growth. Cancer Discov 3: 1105-1107, 2013.
19. Guo D, Tong Y, Jiang X, Meng Y, Jiang H, Du L, Wu Q, Li S, Luo S, Li M, *et al*: Aerobic glycolysis promotes tumor immune evasion by hexokinase2-mediated phosphorylation of IκBα. Cell Metab 34: 1312-1324.e6, 2022.
20. Xu S and Herschman HR: A tumor agnostic therapeutic strategy for hexokinase 1-Null/Hexokinase 2-Positive cancers. Cancer Res 79: 5907-5914, 2019.
21. Zhou QQ, Xiao HT, Yang F, Wang YD, Li P and Zheng ZG: Advancing targeted protein degradation for metabolic diseases therapy. Pharmacol Res 188: 106627, 2023.
22. Ho PW, Leung CT, Liu H, Pang SY, Lam CS, Xian J, Li L, Kung MH, Ramsden DB and Ho SL: Age-dependent accumulation of oligomeric SNCA/α-synuclein from impaired degradation in mutant LRRK2 knockin mouse model of Parkinson disease: Role for therapeutic activation of chaperone-mediated autophagy (CMA). Autophagy 16: 347-370, 2020.
23. Fan X, Jin WY, Lu J, Wang J and Wang YT: Rapid and reversible knockdown of endogenous proteins by peptide-directed lysosomal degradation. Nat Neurosci 17: 471-480, 2014.
24. Zhang S, Williamson NA and Bogoyevitch MA: Complementary proteomics strategies capture an ataxin-1 interactome in Neuro-2a cells. Sci Data 5: 180262, 2018.
25. Xie YC, Dong XW, Wu XM, Yan XF and Xie QM: Inhibitory effects of flavonoids extracted from licorice on lipopolysaccharide-induced acute pulmonary inflammation in mice. Int Immunopharmacol 9: 194-200, 2009.
26. Wang L, Lei W, Zhang S and Yao L: MCC950, a NLRP3 inhibitor, ameliorates lipopolysaccharide-induced lung inflammation in mice. Bioorg Med Chem 30: 115954, 2021.
27. Livak KJ and Schmittgen TD: Analysis of relative gene expression data using real-time quantitative PCR and the 2(-Delta Delta C(T)) method. Methods 25: 402-408, 2001.
28. Wang W, Zheng F, Lin C and Zhang A: Changes in energy metabolism and macrophage polarization: Potential mechanisms of arsenic-induced lung injury. Ecotoxicol Environ Saf 204: 110948, 2020.
29. Fosgerau K and Hoffmann T: Peptide therapeutics: Current status and future directions. Drug Discov Today 20: 122-128, 2015.
30. Leung RK and Whittaker PA: RNA interference: From gene silencing to gene-specific therapeutics. Pharmacol Ther 107: 222-239, 2005.
31. Lin X, Ruan X, Anderson MG, McDowell JA, Kroeger PE, Fesik SW and Shen Y: siRNA-mediated off-target gene silencing triggered by a 7 nt complementation. Nucleic Acids Res 33: 4527-4535, 2005.
32. Castanotto D and Rossi JJ: The promises and pitfalls of RNA-interference-based therapeutics. Nature 457: 426-433, 2009.
33. Yip BH: Recent advances in CRISPR/Cas9 delivery strategies. Biomolecules 10: 839, 2020.
34. Kuscu C, Arslan S, Singh R, Thorpe J and Adli M: Genome-wide analysis reveals characteristics of off-target sites bound by the Cas9 endonuclease. Nat Biotechnol 32: 677-683, 2014.
35. Chen F, Alphonse M and Liu Q: Strategies for nonviral nanoparticle-based delivery of CRISPR/Cas9 therapeutics. Wiley Interdiscip Rev Nanomed Nanobiotechnol 12: e1609, 2020.
36. You L, Tong R, Li M, Liu Y, Xue J and Lu Y: Advancements and obstacles of CRISPR-Cas9 technology in translational research. Mol Ther Methods Clin Dev 13: 359-370, 2019.
37. Behr M, Zhou J, Xu B and Zhang H: In vivo delivery of CRISPR-Cas9 therapeutics: Progress and challenges. Acta Pharm Sin B 11: 2150-2171, 2021.
38. Zhou YF, Wang J, Deng MF, Chi B, Wei N, Chen JG, Liu D, Yin X, Lu Y and Zhu LQ: The Peptide-Directed lysosomal degradation of CDK5 exerts therapeutic effects against stroke. Aging Dis 10: 1140-1145, 2019.
39. O'Neill LA and Pearce EJ: Immunometabolism governs dendritic cell and macrophage function. J Exp Med 213: 15-23, 2016.
40. Li Y, Lu B, Sheng L, Zhu Z, Sun H, Zhou Y, Yang Y, Xue D, Chen W, Tian X, *et al*: Hexokinase 2-dependent hyperglycolysis driving microglial activation contributes to ischemic brain injury. J Neurochem 144: 186-200, 2018.
41. Bao C, Zhu S, Song K and He C: HK2: A potential regulator of osteoarthritis via glycolytic and non-glycolytic pathways. Cell Commun Signal 20: 132, 2022.
42. Yuan Y, Fan G, Liu Y, Liu L, Zhang T, Liu P, Tu Q, Zhang X, Luo S, Yao L, *et al*: The transcription factor KLF14 regulates macrophage glycolysis and immune function by inhibiting HK2 in sepsis. Cell Mol Immunol 19: 504-515, 2022.
43. Qian Y, Chen D, Zhu Y, Wu J, Wang Y and Yang W: Targeting hexokinase 1 alleviates NLRP3-mediated inflammation in apical periodontitis: A laboratory investigation. Int Endod J 56: 734-747, 2023.
44. Qiao L, Ma J, Zhang Z, Sui W, Zhai C, Xu D, Wang Z, Lu H, Zhang M, Zhang C, *et al*: Deficient Chaperone-Mediated autophagy promotes inflammation and atherosclerosis. Circ Res 129: 1141-1157, 2021.
45. Hettwer J, Hinterdobler J, Miritsch B, Deutsch MA, Li X, Mauersberger C, Moggio A, Braster Q, Gram H, Robertson AAB, *et al*: Interleukin-1beta suppression dampens inflammatory leucocyte production and uptake in atherosclerosis. Cardiovasc Res 118: 2778-2791, 2022.
46. Hill MD, Martin RH, Mikulis D, Wong JH, Silver FL, Terbrugge KG, Milot G, Clark WM, Macdonald RL, Kelly ME, *et al*: Safety and efficacy of NA-1 in patients with iatrogenic stroke after endovascular aneurysm repair (ENACT): A phase 2, randomised, double-blind, placebo-controlled trial. Lancet Neurol 11: 942-950, 2012.